

Probing structures in channel flow through SO(3) and SO(2) decomposition

By LUCA BIFERALE^{1,3}, DETLEF LOHSE²,
IRENE M. MAZZITELLI²
AND FEDERICO TOSCHI^{2,3}

¹Department of Physics, University Tor Vergata,
Via della Ricerca Scientifica 1, 00133 Roma, Italy

²Department of Applied Physics and J. M. Burgers Centre for Fluid Dynamics,
University of Twente, P.O. Box 217, 7500 AE Enschede, The Netherlands

³INFM, Unitá di Tor Vergata, Roma, Italy

(Received 26 June 2000 and in revised form 13 July 2001)

SO(3) and SO(2) decompositions of numerical channel flow turbulence are performed. The decompositions are used to probe, characterize, and quantify anisotropic structures in the flow. Close to the wall, the anisotropic modes are dominant and reveal the flow structures. The dominance of the $(j, m) = (2, 1)$ mode of the SO(3) decomposition in the buffer layer is associated with hairpin vortices. The SO(2) decomposition in planes parallel to the walls allows us also to access the regions very close to the wall. In those regions we have found that the strong enhancement of intermittency can be explained in terms of streaklike structures and their signatures in the $m = 2$ and $m = 4$ modes of the SO(2) decomposition.

1. Introduction

Structures called ‘streaks’ have been thought to be the main signatures of wall-bounded flows in the viscous sublayer since the pioneering work of Kline *et al.* (1967) who observed the existence of extremely well-organized motions made of regions of low- and high-speed fluid, elongated downstream and alternating in the spanwise direction. Later, in Kim, Kline & Reynolds (1971), ‘streaks’ were reported to be responsible for turbulent production in the viscous sublayer. Similarly, ‘hairpins’ have been the main persistent structures observed experimentally (Head & Bandyopadhyay 1981; Wallace, Eckelmann & Brodkey 1972) and numerically (Moin & Kim 1985; Kim & Moin 1986) outside the viscous layer, in the turbulent boundary layer. By means of conditional sampling, Kim & Moin (1986) were able to show that these ‘hairpin’ shaped structures are associated with high Reynolds-shear stress and give a significant contribution to turbulent production in the logarithmic layer. For a thorough discussion of structures in wall flow and their characterization with the help of statistical methods see Pope (2000, chap. 7).

How are the structures seen in wall-bounded flows reflected in the statistical theory of turbulence?

Kolmogorov’s classical statistical theory (Kolmogorov 1941) avoids the term structures. He hypothesizes that any turbulent flow isotropizes and homogenizes on the smallest scales. Based on this, he postulates (i) the existence of an inertial range of

scales where (ii) the ‘almost’ isotropic homogeneous turbulent fluctuations are characterized by a power law spectrum with a universal $-\frac{5}{3}$ slope. Both statements are connected and neither is strictly correct. First, it has been established experimentally and numerically (Frisch 1995) that already in the ideal isotropic and homogeneous high-Reynolds-number limit turbulent fluctuations are strongly intermittent. Intermittency means that the probability density of velocity increments, $\delta_{Ru} = (\mathbf{u}(\mathbf{x} + \mathbf{R}) - \mathbf{u}(\mathbf{x})) \cdot \hat{\mathbf{R}}$, cannot be rescaled by using only one single scaling exponent for all distances R , see for example Frisch (1995). Secondly, in almost all relevant applied situations we are interested in those ranges of scales where turbulence statistics are neither homogeneous nor isotropic.

In this paper, as an example, we will discuss the important case of channel flows. Experimental (Garg & Warhaft 1998) and numerical investigations (Pumir & Shraiman 1995; Pumir 1996; Schumacher & Eckhardt 2001) have shown that the tendency towards the isotropization of small-scale statistics of shear flows is much slower than any dimensional prediction, even at very large Reynolds numbers. Even worse, in contrast to what is predicted by the Kolmogorov 1941 theory, some observables such as the skewness of velocity gradients, exhibit persistence of anisotropies.

The two above issues of intermittency and anisotropy are connected. We cannot focus on the issue of intermittency in high-Reynolds-number homogeneous and isotropic statistics without first having a systematic control on the possible slowly decaying anisotropic effects that are always present in all numerical or experimental investigations. Similarly, the understanding of complex non-homogeneous and anisotropic flows cannot avoid the problem of intermittent isotropic and anisotropic fluctuations.

Toschi *et al.* (1999) and Benzi *et al.* (1999) started a systematic investigation of the intermittent properties of velocity increments parallel to the wall as a function of the distance from the wall in a channel-flow simulation. In this case, a clear transition between the bulk physics and the wall physics was recognized in terms of two different sets of intermittent exponents characterizing velocity fluctuations at the centre and close to the channel walls. A firm quantitative understanding of how much these intermittent quantifiers can be connected to the presence of persistent structures is still lacking. For instance, in Benzi *et al.* (1999), the different behaviour of velocity fluctuations in the buffer layer was explained as a breaking of the Kolmogorov refined hypothesis linking energy dissipation to inertial velocity fluctuations, i.e. an effect due to the different production and dissipation mechanism caused by the presence of strong shear effects close to the walls. Clearly, such an issue can only be addressed by using systematic tools which are able to quantify the degree of anisotropy and coherency at different scales and at different spatial locations in the flow.

In this paper, we suggest as such a tool the exact decompositions of the correlation functions in terms of the irreducible representations of the rotational group $SO(3)$ (in the bulk of the flow) and in terms of the irreducible representation of the two-dimensional rotational group $SO(2)$ (close to the walls). The $SO(3)$ decomposition has been introduced by Arad *et al.* (1998, 1999*a,b*) and meanwhile used extensively (Grossmann, Lohse & Reeh 1998; Kurien *et al.* 2000; Grossmann, von der Heydt & Lohse 2001; Kurien & Sreenivasan 2001*a,b*). With this tool, we can quantify in a systematic way the relative and absolute degree of anisotropy of velocity fluctuations. The $SO(3)$ decomposition, being connected to the exact invariance under rotations of the inertial and diffusive terms of the Navier–Stokes equations, can disentangle universal scaling properties of the isotropic sectors from the more complex behaviour in the anisotropic sectors. We also show how the $SO(2)$ decompositions in planes

parallel to the walls are useful analysing tools in order to quantify the relative change of planar anisotropy when approaching the boundaries.

Furthermore, we show how a statistical data analysis, in principle, allows for a connection between some coefficients of the decompositions and the ‘structures’ observed by simple flow visualization. We therefore try to contribute to filling the gap between the quantitative systematic methodology used in ‘ideal’ homogeneous and isotropic turbulence and the more qualitative description in terms of ‘structures’ used in the ‘non-ideal’ wall-bounded flows.

The paper is organized as follows. In §2, we review the main theoretical considerations about the importance of the SO(3) decomposition in the Navier–Stokes equations. In §3, we present a systematic analysis of the SO(3) decomposition in a numerical channel flow database. We discuss the results with particular emphasis on the universality issue, i.e. independence from the large-scale effects, and on how we can use such a decomposition to quantify the relative importance of structures such as ‘hairpin’ in the bulk of the flow. In §4, we present the results from the SO(2) decompositions in planes well inside the buffer layer, i.e. where the SO(3) decomposition cannot be applied owing to the presence of the rigid walls. In particular, we show how the SO(2) analysis allows us to distinguish clearly the existence of ‘streak’ like structures in a statistical sense. Section 5 contains comments and conclusions.

2. SO(3) decomposition

SO(3)–rotational invariance–is one of the basic symmetries of the Navier–Stokes equations. However, it is broken by the boundary conditions or by the driving force of the flow, both of which introduce anisotropy and also inhomogeneities. Let us start, as an example, with the SO(3) decomposition of the second-order velocity correlation depending only on one spatial increment \mathbf{R} :

$$C_{\alpha\beta}(\mathbf{x}, \mathbf{R}) = \langle (u_\alpha(\mathbf{x} + \mathbf{R}) - u_\alpha(\mathbf{x}))(u_\beta(\mathbf{x} + \mathbf{R}) - u_\beta(\mathbf{x})) \rangle. \quad (2.1)$$

This observable can be decomposed in terms of the irreducible representations of the three-dimensional rotational group (Arad *et al.* 1999b) which form a complete basis in the space of smooth second-order tensors depending on one vector \mathbf{R} :

$$C_{\alpha\beta}(\mathbf{x}, \mathbf{R}) = \sum_{qjm} a_{q,jm}(\mathbf{x}, R) B_{\alpha\beta}^{q,jm}(\hat{\mathbf{R}}). \quad (2.2)$$

The notation in (2.2) is borrowed from the quantum mechanical analogue, i.e. $j = 0, 1, \dots$ labels the eigenvalues of the modulus of the total angular momentum \mathbf{L}^2 ; $m = -j, \dots, +j$ labels the eigenvalues of the projection of the total angular momentum in one direction, say \hat{y} ; q labels the different irreducible representations corresponding to a given j ; and $B_{\alpha\beta}^{q,jm}(\hat{\mathbf{R}})$ are the eigenfunctions of the rotational group in the space of second-order smooth tensors; they only depend on the $\hat{\mathbf{R}} = \mathbf{R}/R$. For the fully isotropic sector, $j = 0$, we have only $m = 0$, and a simple calculation shows that there are only two independent irreducible representations in the isotropic sector, i.e. the well-known result (Monin & Yaglom 1975) that we need only two independent eigenfunctions in order to describe any second-order isotropic tensor. These two eigenfunctions can be taken to be:

$$B_{\alpha\beta}^{1,00}(\hat{\mathbf{R}}) = \delta_{\alpha,\beta}, \quad B_{\alpha\beta}^{2,00}(\hat{\mathbf{R}}) = \hat{\mathbf{R}}_\alpha \hat{\mathbf{R}}_\beta,$$

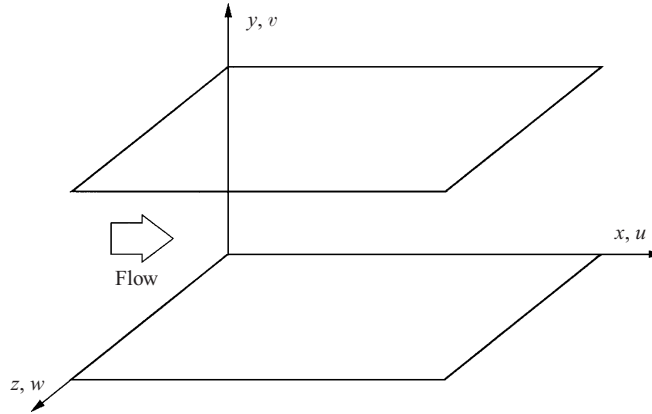


FIGURE 1. Coordinate system in channel. Shown are streamwise (x), spanwise (z), and wall-normal (y) directions.

and therefore the decomposition (2.2) in the isotropic sector assumes the familiar form

$$C_{\alpha\beta}(\mathbf{x}, \mathbf{R}) = a_{1,00}(\mathbf{x}, R)\delta_{\alpha,\beta} + a_{2,00}(\mathbf{x}, R)\hat{\mathbf{R}}_{\alpha}\hat{\mathbf{R}}_{\beta}. \quad (2.3)$$

In the Appendix we list the complete set of $B_{\alpha\beta}^{q,jm}$ for the case of second-order tensors. For higher tensor ranks we refer to Arad *et al.* (1999b). The main physical information is, of course, hidden in the dependence of the coefficients $a_{q,jm}(\mathbf{x}, R)$ on the spatial location, \mathbf{x} , and on the analysed scale, R . We aim to use the decomposition (2.2) as a filter able to disentangle different anisotropic effects as a function of the spatial location and of the analysed scale. In previous studies, the main interest was focused on the theoretical issue of the existence of scaling behaviour for the coefficients $a_{q,jm}(\mathbf{x}, R)$ and on its possible dynamical explanation in terms of the ‘foliation’ of the Navier–Stokes equations in different j sectors (Arad *et al.* 1998, 1999a,b; Biferale & Toschi 2001; Grossmann *et al.* 2001). The typical questions addressed were whether coefficients belonging to different j sectors have different scaling behaviour (if any) and, in this case, which kind of dimensional estimate for scaling exponents in the anisotropic sectors we could propose. As for the issues of scaling behaviour, owing to the limitation of small Reynolds numbers in the numerical case (Arad *et al.* 1999a; Biferale & Toschi 2001), and to the limited amount of information available on the tensorial structure of the velocity field in the experimental case (Arad *et al.* 1998; Kurien *et al.* 2000; Kurien & Sreenivasan 2001), only partial answers have been found. Among them, the most important is the strong universality shown by the isotropic sector as a function of the local degree of non-homogeneity (and anisotropy), i.e. the independence on \mathbf{x} shown by the scaling properties of the coefficients $a_{q,00}(\mathbf{x}, R)$ in non-homogeneous turbulence (Arad *et al.* 1999a).

In this paper, we do not focus on possible scaling behaviour but we would like to suggest the SO(3) decomposition as an appropriate tool to analyse, characterize, and quantify the non-universal large-scale geometric properties of the turbulent flow. As an example, we take numerical channel flow (Amati, Succi & Piva 1997; Toschi *et al.* 1999) obtained by a lattice Boltzmann code running on a massively parallel machine. The spatial resolution of the simulation is $256 \times 128 \times 128$ grid points. Periodic boundary conditions were imposed along the streamwise (x) and spanwise (z) directions, whereas no-slip boundary conditions were applied at the top and at

the bottom planes (y -direction) (see figure 1). The Reynolds number at the centre of the channel is about 3000.

We assume that, owing to the homogeneity in planes parallel to the walls, there is only a dependence on the height y of all statistical observables. The coefficients $a_{q,jm}(\mathbf{x}, R)$ carry two types of information: (i) their scaling behaviour $a_{q,jm}(\mathbf{x}, R) \propto R^{\zeta_{q,jm}^{(2)}}$ which at least for small scales and large Re is hoped to be universal, i.e. position and flow independent[†], and (ii) their absolute or relative magnitudes which clearly are non-universal, i.e. position \mathbf{x} and flow-type dependent. These ratios characterize what kinds of structure the flow contains. These are time- and ensemble-averaged quantities, obeying the underlying Navier–Stokes SO(3) symmetry, and we consider them to be a more systematic tool for structure characterization than snapshots of vortex sheets, worms, swirls or contour plots of either the velocity or the vorticity fields.

When analysing higher-order structure tensors $C_{\alpha\beta\dots\gamma}(\mathbf{x}, \mathbf{R})$, the decomposition of type (2.2) soon becomes cumbersome. Moreover, in most experiments, the full tensorial information is not available. Therefore, we are restricted to an abbreviated form of the SO(3) decomposition of the velocity structure tensor, namely, the SO(3) decomposition of the longitudinal structure function. In this case, the undecomposed observable is a scalar under rotations and there exists only one irreducible representation for each j sector, i.e. the usual spherical harmonics basis set $Y_{jm}(\hat{\mathbf{R}})$. We have to be careful, however, as using only scalar quantities may not be enough to fully characterize the geometrical contents of statistically important structures. We decompose the longitudinal structure function

$$S_L^{(p)}(\mathbf{x}, \mathbf{R}) = \left\langle \left((\mathbf{u}(\mathbf{x} + \mathbf{R}) - \mathbf{u}(\mathbf{x} - \mathbf{R})) \cdot \hat{\mathbf{R}} \right)^p \right\rangle, \quad (2.4)$$

as follows:

$$S_L^{(p)}(\mathbf{x}, \mathbf{R}) = \sum_{jm} S_{jm}^{(p)}(\mathbf{x}, R) Y_{jm}(\hat{\mathbf{R}}). \quad (2.5)$$

We expect that when scaling behaviour sets in (presumably at high enough Re , far beyond what we can achieve in numerical simulations) we should find:

$$S_{jm}^{(p)}(\mathbf{x}, R) \sim a_{jm}(\mathbf{x}) R^{\zeta_{jm}^{(p)}}. \quad (2.6)$$

Again, the $S_{jm}^{(p)}(\mathbf{x}, R)$ carry both the scaling information $S_{jm}^{(p)}(\mathbf{x}, R) \propto R^{\zeta_{jm}^{(p)}}$ and their non-universal amplitudes.

A practical problem with the decomposition (2.5) of (2.4) is that for \mathbf{x} close to the boundaries, the scale R is restricted to lengths smaller than the distance from the wall, and the large scales cannot be probed. Therefore, we will also perform a decomposition of (2.4) which obeys the weaker SO(2) symmetry, i.e. rotational invariance in a plane for fixed distance y from the wall,

$$D_L^{(p)}(y, \mathbf{R}) = \sum_m d_m^{(p)}(y, R) \exp(im\phi). \quad (2.7)$$

The orientation dependence in a plane reduces to the dependence on an angle ϕ . Again, the $d_m^{(p)}(y, R)$ carry both scaling and amplitude information.

Let us notice at this point that the SO(3) decomposition has its roots on the intimate

[†] The issue of universality of sectors with $j > 0$ is far from being trivial. A lack of universality may be due to the existence of infrared (IR) or ultraviolet (UV) divergences in the non-local integral induced by the pressure terms in the Navier–Stokes equations (Arad *et al.* 1998).

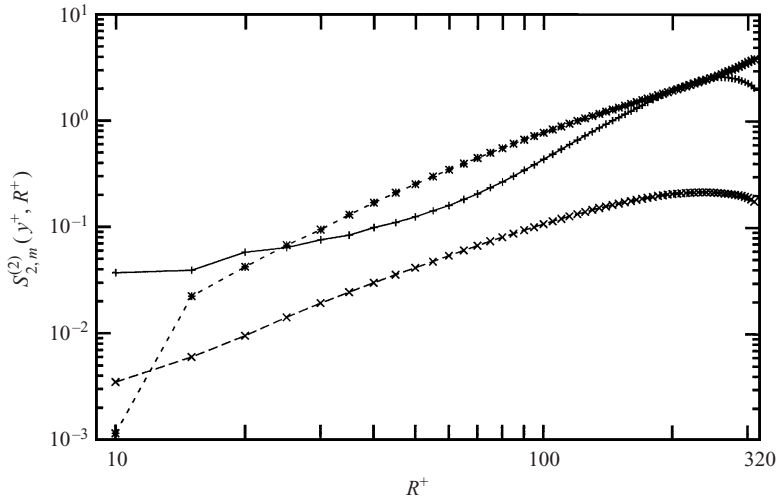


FIGURE 2. Log-log plot of $S_{2,2}^{(2)}(y^+, R^+)$ (*), $S_{2,1}^{(2)}(y^+, R^+)$ (\times), and $S_{2,0}^{(2)}(y^+, R^+)$ (+) as functions of R^+ at the centre of the channel $y^+ = 160$.

structure of the Navier–Stokes equations, i.e. on the invariance under rotations of the inertial and dissipative terms and on the relative foliations on different sectors of the three-dimensional rotational group of the equation of motion of any correlation function (Arad *et al.* 1999*b*). For two-dimensional observables, no such closed equation exists. Nevertheless, the $SO(2)$ decomposition can still be seen as a powerful tool to exactly decompose any observable in a fixed plane as a function of isotropic and anisotropic structures in the plane itself.

3. $SO(3)$ analysis of a turbulent channel flow field

In previous studies, most of the attention was paid to the isotropic sector of the structure function decomposition (2.5), i.e. on the behaviour of $S_{00}^{(p)}(\mathbf{x}, R)$ as a function of the centre of the decomposition \mathbf{x} and of the scale R . In Arad *et al.* (1999*a*), it was shown that the isotropic projection enjoys much better scaling properties than the undecomposed structure function and that these properties are robust with respect to the changing of the local degree of anisotropy, i.e. with respect to the centre of the decomposition, \mathbf{x} . These findings support the idea of universality of the isotropic scaling exponents. It was possible to say very little about scaling of the anisotropic sectors because of lack of spatial resolution; the only qualitative statement was that the scaling exponent of the $j = 2$ sector was roughly $\frac{4}{3}$, as predicted by the dimensional argument given by Lumley (1967) or by Grossmann *et al.* (1994).

3.1. $SO(3)$ decomposition and structures

Here we concentrate on the more applied question of how much the different projections, independently of their possible scaling properties, can teach us about the preferred geometrical structures present in the flow when changing the analysing position in the channel.

In figures 2 and 3 we present the three different contributions we have in the $j = 2$ non-isotropic sector extracted at the centre of the channel ($y^+ = 160$) and at a quarter ($y^+ = 80$), respectively. (The $j = 1$ sector is absent owing to the symmetries of the structure functions chosen in this work.) From now on, with the notation y^+

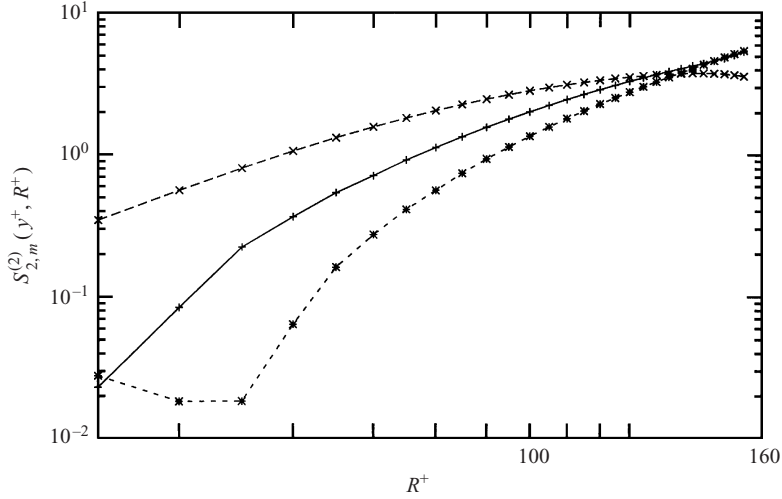


FIGURE 3. Log-log plot of $S_{2,2}^{(2)}(y^+, R^+)$ (*), $S_{2,1}^{(2)}(y^+, R^+)$ (\times), and $S_{2,0}^{(2)}(y^+, R^+)$ (+) as functions of R^+ at $y^+ = 80$.

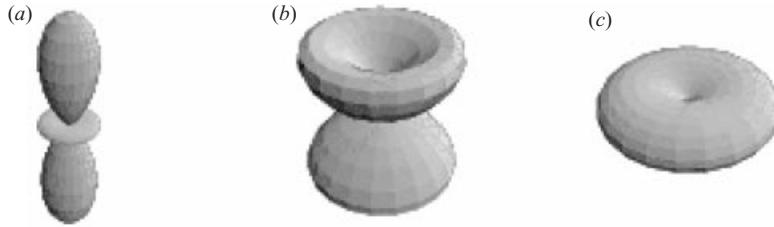


FIGURE 4. Graphical representation of spherical harmonics (a) $|Y^{2,0}(\theta, \phi)|$, (b) $|Y^{2,1}(\theta, \phi)|$, and (c) $|Y^{2,2}(\theta, \phi)|$.

we mean normalization with respect to the wall coordinates. The relative size of the $S_{2m}^{(2)}(y^+, R^+)$ for different m and fixed y^+ characterizes the geometry of the anisotropic structures on the corresponding scale R . Note also that the distance at which velocity increments are measured (R) is normalized to wall units (R^+). For $y^+ = 80$, the ($j = 2, m = 1$) mode is very pronounced on smaller scales, see figure 3. We associate this with the hairpin vortices and other structures which diagonally detach from the wall and which are projected out by Y_{21} . For a visualization of Y_{2m} see figure 4. In the centre, the ($j = 2, m = 1$) mode is two orders of magnitude less pronounced than at $y^+ = 80$. Our interpretation is that the diagonal structures from above and below have equal and opposite contributions.

The most pronounced structures in the centre are those parallel to the flow direction, i.e. ($j = 2, m = 2$), see figure 2. Also at $y^+ = 80$ the structures parallel to the flow direction (mode ($j = 2, m = 2$)) are rather pronounced. At scales beyond $R^+ \approx 100$ they overwhelm the diagonal contributions (mode ($j = 2, m = 1$)). Therefore, we are tempted to interpret $R^+ \approx 100$ as the typical maximal size of the hairpin vortices.

We repeated this type of analysis for the $S_{2m}^{(4)}(y^+, R^+)$ with very similar results.

3.2. Higher-order moments and the lack of isotropy at small scales

The first question we may want to ask about the decomposition (2.5) is whether it converges with increasing j . We want to check this for an R in the streamwise flow

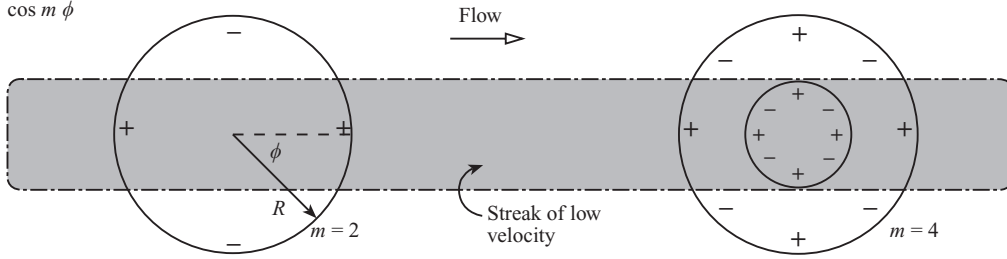


FIGURE 5. Sketch of a 'streak' in an (x, z) plane probed with the $m = 2$ and $m = 4$ eigenfunctions.

direction, i.e. $\hat{\mathbf{R}} = (\theta, \phi) = (\frac{1}{2}\pi, 0)$. As we can see from figure 6(a), at small scales and in the channel centre, where anisotropic contributions are small, the convergence is good; but away from the centre ($y^+ = 62$) and in particular for large scales, the quality of the convergence becomes poor, see figure 6(b). Note that in any case the convergence is not monotonous as a function of the scale.

Another, even more informative way to quantify the rate of isotropization is to plot the ratio of each single amplitude $S_{jm}^{(2)}(\mathbf{x}, \mathbf{R})$ to the total structure function $S_L^{(2)}(\mathbf{x}, \mathbf{R})$ with \mathbf{R} in the direction of the mean flow. In figures 7(a) and 7(b), we can find the above quantities at the centre of the channel $y^+ = 160$ and in the buffer layer $y^+ = 62$, respectively. At large scales there are contributions from all resolved j sectors indicating, as already seen above, a lack of convergence of the decomposition at those scales.

In the buffer layer, the relative ratio of the anisotropic sectors is much higher than what is seen in the centre. Moreover, even more interestingly, in the buffer layer, where owing to the presence of a high shear we can imagine a statistically stable signature of anisotropic physics, there appears to be a clear grouping of different sectors labelled by different j indices: Figure 7(b) shows that projections with the same j but different m indices have a qualitative similar behaviour. Of course, this kind of comparison depends on the direction of the undecomposed structure functions (here taken parallel to the walls).

Another test of the relative weights of anisotropies (now independent of the chosen coordinate system) is to plot the ratio between the isotropic projection $S_{00}^{(p)}(\mathbf{x}, \mathbf{R})$ and the other anisotropic projections for $j > 0$. Such a test is carried out in terms of quantities depending only on the separation magnitude R , and therefore measures the relative importance of anisotropies independently of the orientation. In figure 8 we show, for example, the ratio between the sector $(j, m) = (4, 4)$ and the isotropic sector $(j, m) = (0, 0)$ as a function of the wall distance and the scale R^+ . As expected, by approaching the wall (decreasing y^+), the ratio becomes larger and larger, showing clearly the importance of high j fluctuations in the sheared buffer layer.

This convergence analysis is a systematic quantitative way of understanding the rate of isotropization toward small scales exhibited by this particular flow as a function of the distance from the wall. However, the lack of convergence of the SO(3) decomposition close to the wall also shows its limitations once highly anisotropic structures are present; many (j, m) -amplitudes are necessary to characterize them.

All the previous trends have also been found, amplified, by analysing higher moments. For example, in figures 9(a) and 9(b) we re-plot the same terms as in figures 7(a) and 7(b) but for the fourth-order structure functions. The fact that the previous trends are much more enhanced for higher-order moments is an indication

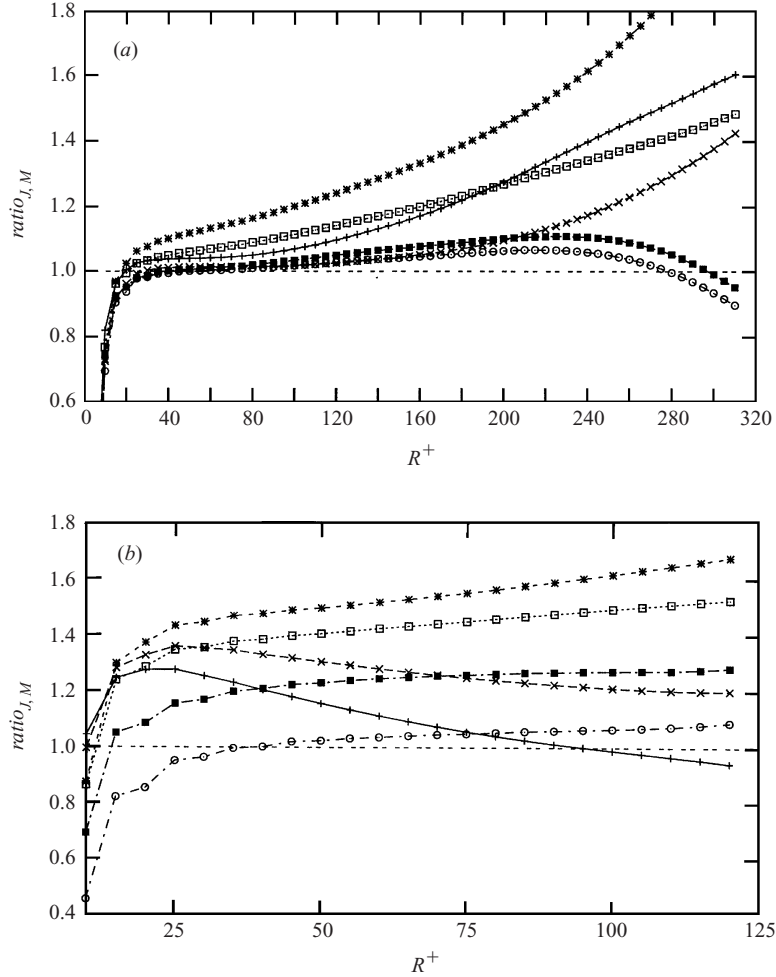


FIGURE 6. Analysis of the convergence of the SO(3) decomposition: $ratio_{J,M}$ represents the ratio between the longitudinal structure function of order 2 in the streamwise direction reconstructed up to $(J, M) = (0, 0)$ (+), $(J, M) = (2, 0)$ (x), $(J, M) = (2, 2)$ (*), $(J, M) = (4, 0)$ (□), $(J, M) = (4, 2)$ (■), and $(J, M) = (4, 4)$ (○) and the undecomposed structure function, (a) at the centre of the channel $y^+ = 160$ and (b) at $y^+ = 62$.

that anisotropy fluctuations are important but ‘rare’, i.e. are connected to intense fluctuations in a sea of isotropic turbulence.

4. SO(2) analysis of a turbulent channel flow

As discussed in the previous sections, the SO(3) decomposition turned out to be useful as it is able to highlight statistical information as a function of geometrical structures. However, the SO(3) decomposition suffers from some drawbacks when we want to analyse the statistical turbulent behaviour close to the fluid boundaries. They originate from the need to perform integrals over a given sphere, and therefore close to the boundaries the limitation of the sphere radius does not allow us to extract any information except for a very limited (almost fully dissipative) range of scales.

To overcome this problem, we propose to use a decomposition in eigenfunctions of the group of rotations in two dimensions, SO(2). The rationale behind this idea

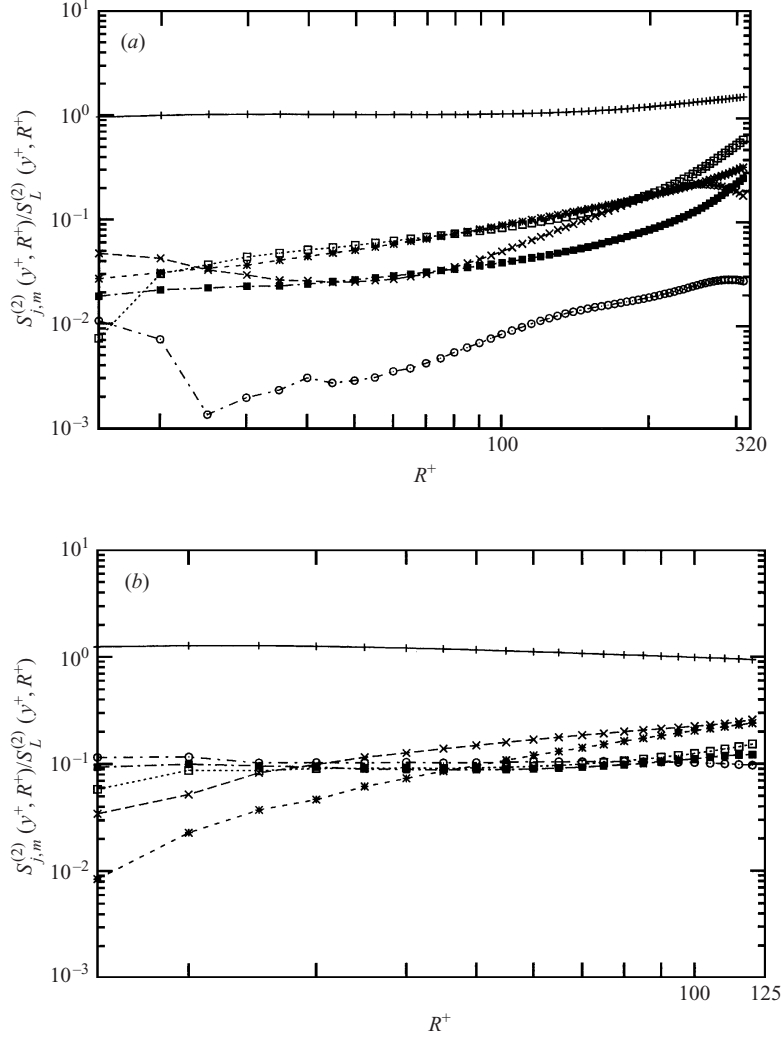


FIGURE 7. Ratio of each single (j, m) amplitude $S_{j,m}^{(2)}(y^+, \mathbf{R})$ to the total structure function $S_L^{(2)}(y^+, \mathbf{R})$ with \mathbf{R} in the direction of the mean flow and (a) $y^+ = 160$, (b) $y^+ = 62$. The (j, m) indices are: $(0, 0)$ (+), $(2, 0)$ (\times), $(2, 2)$ (*), $(4, 0)$ (\square), $(4, 2)$ (\blacksquare), and $(4, 4)$ (\circ).

is that the Navier–Stokes equations obviously obey the $SO(2)$ symmetry and for the channel flow also the geometry obeys this symmetry, once the rotation axis is chosen in the y -direction. However, the mean flow breaks the $SO(2)$ symmetry as it breaks the $SO(3)$ symmetry. Nevertheless, we will gain a tool that is able to exactly decompose any two-dimensional observable in terms of fluctuations with a given property under two-dimensional rotations. In the region very close to the walls where very elongated ‘streak’ structures have been observed, the $SO(2)$ analysis may help in understanding the relative importance of isotropic and anisotropic planar fluctuations.

4.1. $SO(2)$ decomposition and structures

The $SO(2)$ decomposition of the longitudinal structure function $D_L^{(p)}(y, \mathbf{R})$ is defined as

$$D_L^{(p)}(y, \mathbf{R}) = \sum_m d_m^{(p)}(y, \mathbf{R}) \exp(im\phi), \quad (4.1)$$

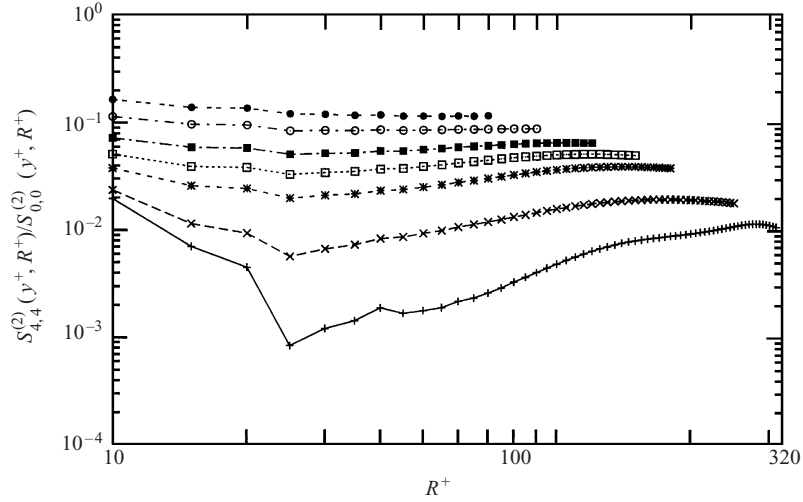


FIGURE 8. Ratios between the sector $(j, m) = (4, 4)$ of the decomposition of $S_L^{(2)}(y^+, R^+)$ and the isotropic sector $(j, m) = (0, 0)$ as functions of R , on changing the analysed height in the channel: $y^+ = 160$ (+), $y^+ = 125$ (×), $y^+ = 92$ (*), $y^+ = 80$ (□), $y^+ = 62$ (■), $y^+ = 48$ (○), and $y^+ = 37$ (●).

where \mathbf{R} is a two-dimensional vector lying in a plane at fixed y . Owing to the symmetry of the structure function only even values of m will contribute to the sum in (4.1).

In figures 10(a) and 10(b) we show the rate of convergence of the reconstructed structure function of order 2 as a function of the maximum M contributing to the right-hand side of (4.1) and at two different distances from the wall, at the centre (figure 10a) and in the buffer layer (figure 10b). The findings are the same as for the SO(3) decomposition. (i) In the centre of the channel, we find a good convergence. (ii) However, in the buffer layer, even when reaching $M = 8$, large scales are still far from being reconstructed. This reflects the tendency of the formation of large and intense anisotropic structures. These trends are even more pronounced for the fourth-order moment as shown in figures 11(a) and 11(b).

In figure 12(a) we show the absolute weight of different m -contributions for the second-order structure function, again in the centre. Note that there is a clear monotonic organization of different contributions as a function of their isotropic/anisotropic properties, i.e. higher values of m are less intense than lower values of m in a systematic way at all scales.

In contrast, in the buffer layer, figure 12(b), there is a crossing of the $m = 2$ contribution and of the $m = 4$ contribution at scales of the order of $R^+ \sim 90$. We interpret this crossing as the signature of the formation of structures or streaks with typical width $R^+ \sim 90$ and with a preferred orientation projected out by the $m = 4$ eigenfunction; the $m = 2$ eigenfunction weighs essentially the difference between velocity correlations in the streamwise and in the spanwise directions, whereas those contributions *sum* in the projection on the $m = 4$ eigenfunction (see figure 5). Thus, at scales R^+ smaller than the typical streak width, the intensity of the $m = 4$ coefficient will exceed that of the $m = 2$ coefficient. On the other hand, at large scales $R^+ > 90$, we find the normal ordering $d_0^{(2)}(37, R^+) > d_2^{(2)}(37, R^+) > d_4^{(2)}(37, R^+) > d_6^{(2)}(37, R^+)$. That elongated structures exist close to the wall is shown in the contour plot of figure 13, and of course is known from many experiments and simulations (see Pope 2000, chap. 7).

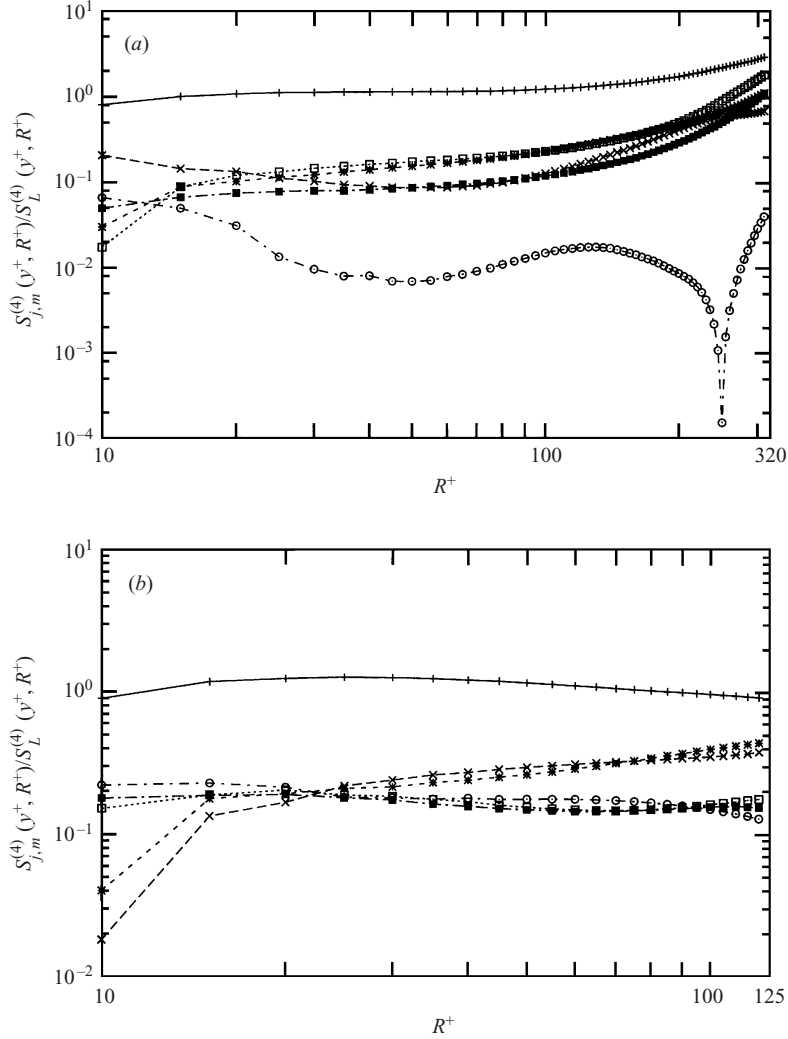


FIGURE 9. Ratio of each single (j, m) amplitude $S_{j,m}^{(4)}(y^+, \mathbf{R})$ to the total structure function $S_L^{(4)}(y^+, \mathbf{R})$ with \mathbf{R} in the direction of the mean flow and (a) $y^+ = 160$, (b) $y^+ = 62$. The (j, m) indices are: $(0, 0)$ (+), $(2, 0)$ (\times), $(2, 2)$ (*), $(4, 0)$ (\square), $(4, 2)$ (\blacksquare), and $(4, 4)$ (\circ).

The above trends are again more intense for $p = 4, 6, \dots$. For $p = 6$, the dominant contribution at large scales (not shown) is given by the $m = 2$ sector, proving, once more, the extreme departure from isotropy (in the plane) close to the walls.

In order to quantify the departure from isotropy in each plane at a changing distance from the wall, we plot the ratios between the projections on the $m = 2$ sector and the isotropic sector (figure 14a) at a varying distance from the wall and for some R^+ values. Figure 14(b) shows the same but for $m = 4$. Note the sharp transition at $y^+ \sim 40$ from almost isotropic statistics ($y^+ > 40$) to strongly anisotropic statistics ($y^+ < 40$); this is again the signature of the beginning of the buffer layer with ‘structures’. The ratio of the anisotropic to the isotropic amplitudes peaks around $y^+ = 10$. In the viscous sublayer $y^+ < 10$, the anisotropy loses importance.

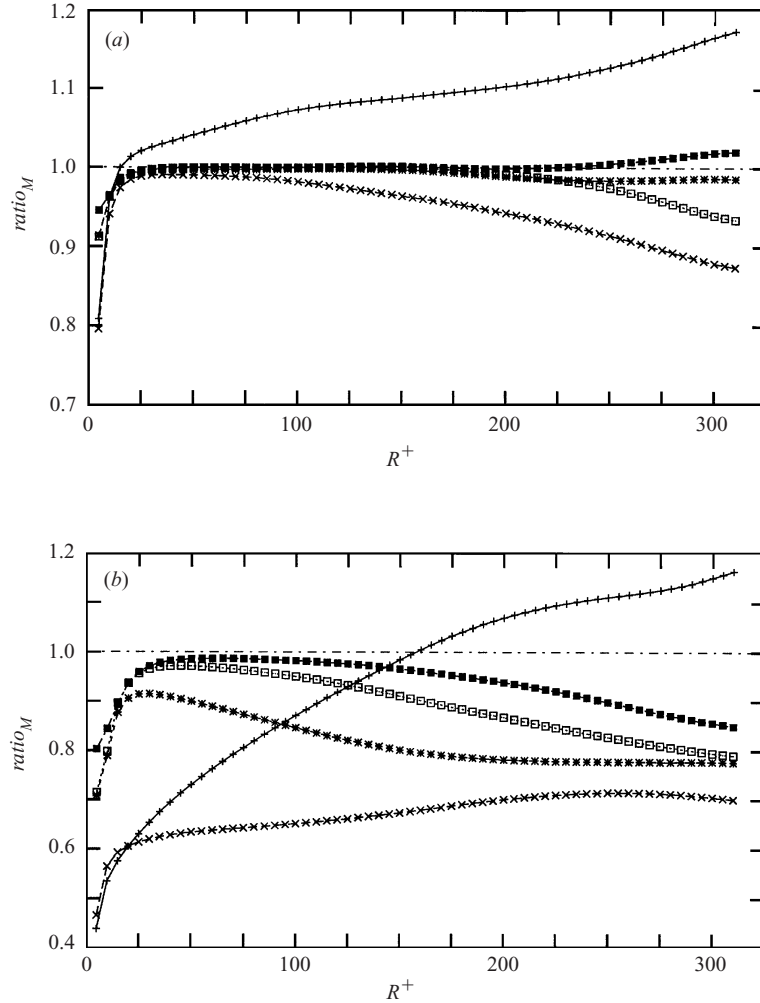


FIGURE 10. Analysis of the convergence of the SO(2) decomposition: $ratio_M$ represents the ratio between the longitudinal structure function of order 2 in the streamwise direction reconstructed up to $M = 0$ (+), $M = 2$ (×), $M = 4$ (*), $M = 6$ (□), and $M = 8$ (■) and the undecomposed structure function, (a) at the centre of the channel $y^+ = 160$ and (b) at $y^+ = 37$.

4.2. Extended self-similarity plots for SO(2) decomposed structure functions

Let us now switch to the more statistically minded question of the experimental and numerical finding of stronger intermittency corrections close to the walls (Benzi, Struglia & Tripiccone 1996b; Gaudin *et al.* 1998; Toschi *et al.* 1999, 2000; Onorato, Camussi & Iuso 2000). Remarkably, these corrections display universality, i.e. the same exponents were measured in different set-ups. This result has been connected with a universal shear-dominated range for scales R larger than the shear length $L_{\mathcal{G}} = (\varepsilon/\mathcal{G}^3)^{1/2}$. In that range, we can expect different energy transfer statistics and as a consequence the breakdown of Kolmogorov's refined similarity hypothesis.

Can we see the features of this shear-dominated universality class of intermittency also in the wall region of the present channel flow? In order to extract any quantitative information on scaling exponents in numerical simulations we must use the ESS

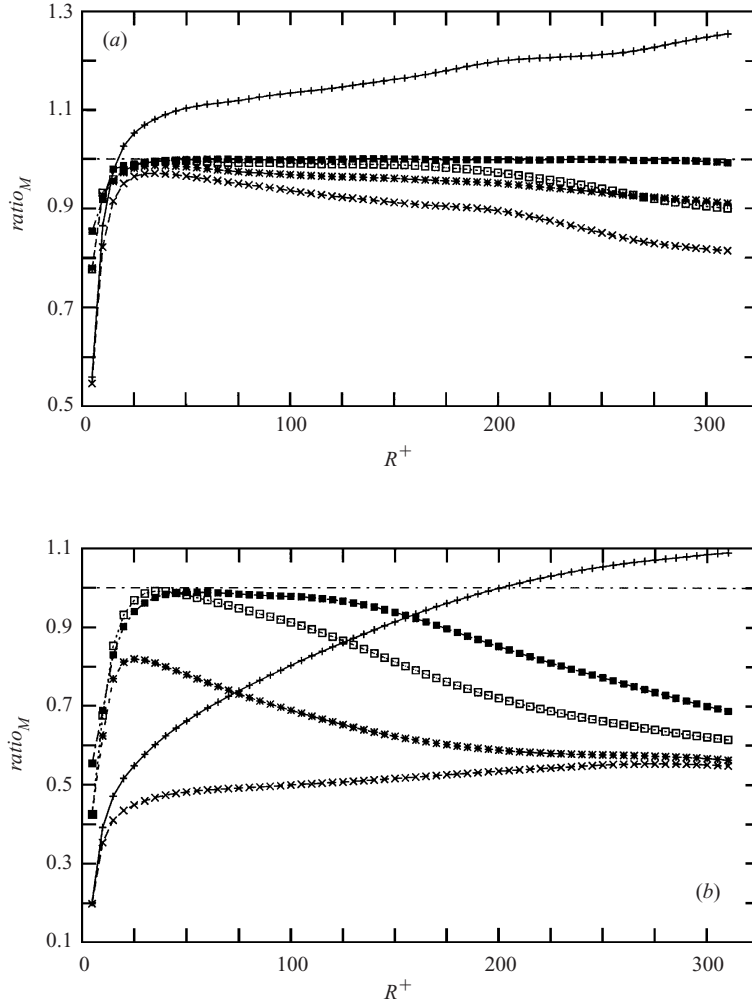


FIGURE 11. Analysis of the convergence of the SO(2) decomposition: $ratio_M$ represents the ratio between the longitudinal structure function of order 4 in the streamwise direction reconstructed up to $M = 0$ (+), $M = 2$ (x), $M = 4$ (*), $M = 6$ (\square), and $M = 8$ (\blacksquare) and the undecomposed structure function, (a) at the centre of the channel $y^+ = 160$ and (b) at $y^+ = 37$.

technique (Benzi *et al.* 1993, 1996a; Grossmann, Lohse & Reeh 1997). ESS is based on the experimental and numerical observation that structure functions even at moderate Reynolds numbers show scaling in a generalized sense, i.e. they scale when plotted against each other. In particular, we want to analyse the scaling:

$$D_L^{(p)}(y, R) \sim \left(D_L^{(2)}(y, R) \right)^{\zeta^{(p)}(y)/\zeta^{(2)}(y)}. \quad (4.2)$$

Here, we have limited ourselves again to the analysis of structure functions in the plane. In (4.2), we have explicitly taken into account the possibility that the scaling exponents depend on the distance from the walls. As stated above, Toschi *et al.* (1999) have shown that there exist two distinct sets of exponents: one governing the scaling in the range of scales smaller than $L_{\mathcal{S}}$ (i.e. close to the centre of the channel, in our case) which is given in terms of the usual isotropic and homogeneous set of

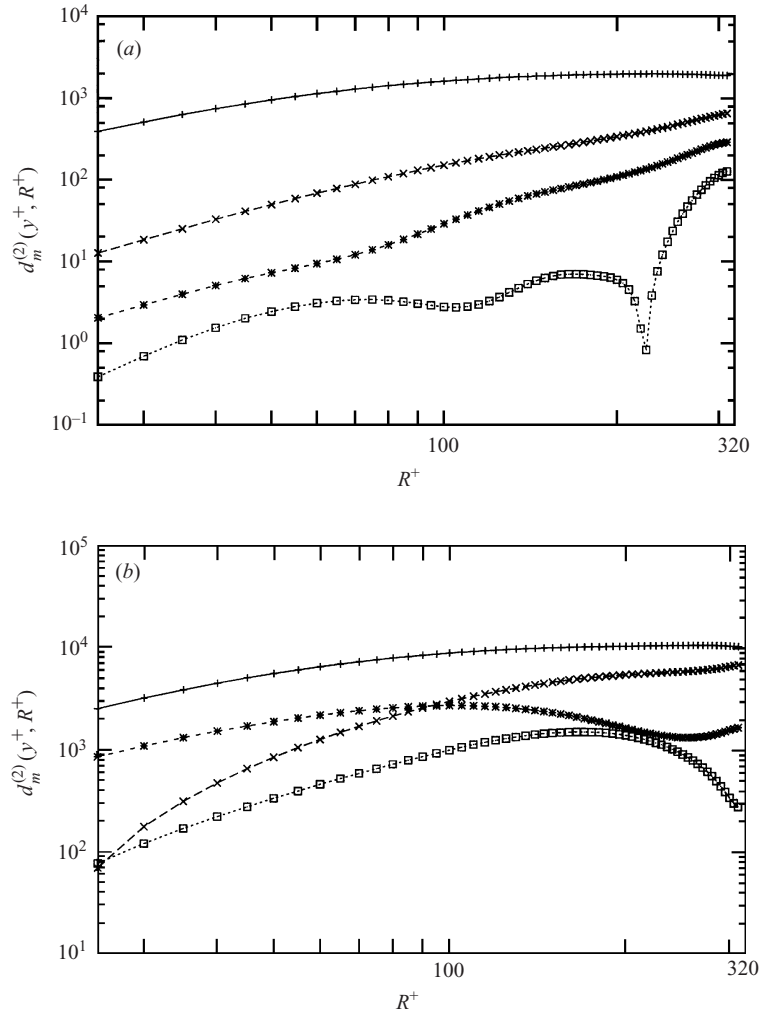


FIGURE 12. Absolute weight of different $d_m^{(p)}(y^+, R^+)$ contributions for the second-order structure function (a) at the centre of the channel $y^+ = 160$ and (b) in the buffer layer at $y^+ = 37$. The m values of these components are: 0 (+), 2 (x), 4 (*), and 6 (\square).

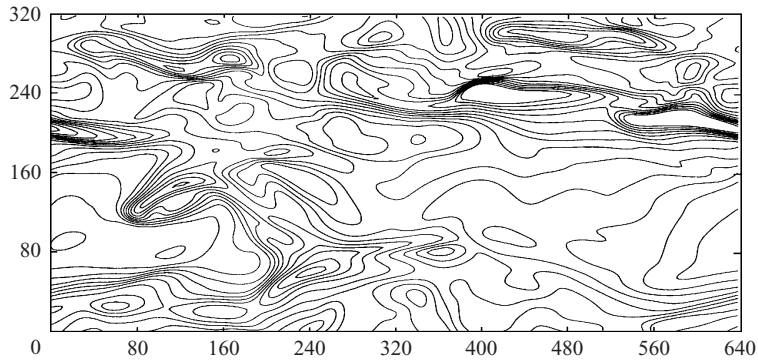


FIGURE 13. Contour plot of the fluctuations of the streamwise velocity at $y^+ = 37$.

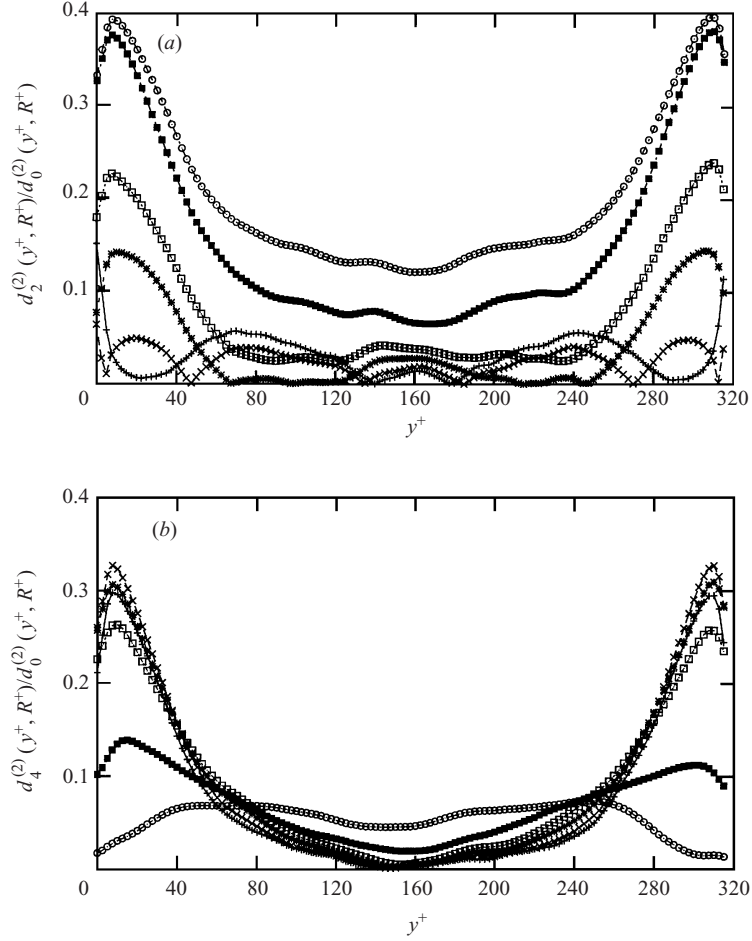


FIGURE 14. Ratio between the projection on (a) the $m = 2$ sector and (b) the $m = 4$ sector, and on the isotropic sector $m = 0$ as a function of y^+ , for $R^+ = 10$ (+), 25 (\times), 50 (*), 75 (\square), 150 (\blacksquare), and 250 (\circ).

exponents; and the second one governing the scaling in the shear dominated range of scales $R > L_{\mathcal{G}}$ (i.e. close to the walls in our channel simulation).

In figure 15 we show the ESS local slopes of the undecomposed structure function in the streamwise direction in the centre of the channel and the same for the projection on the $m = 0$ sector for the moments $p = 2$ versus $p = 4$. Already the fully isotropic component (in the plane) is able to reproduce well the undecomposed observable and both are in good agreement with the isotropic and homogeneous scaling. This finding confirms that at the centre of the channel the whole range of scales is affected only weakly by any shear effect, reflecting that here $R \ll L_{\mathcal{G}}$, which diverges to infinity at the channel centre. On the other hand, in figure 16 we show the same quantities as in figure 15 but now in a plane well inside the buffer layer ($y^+ = 37$). Here, the $m = 0$ component does not reproduce the undecomposed observable, confirming the anisotropy. However, remarkably, it is enough to add the $m = 2$ sector, i.e. to reconstruct up to $M = 2$ in the right-hand side of (4.1), to have good agreement with the more intermittent undecomposed structure function local slope. This is evidence that, as far as the new scaling properties are concerned, the main effect is brought by the $m = 2$ ‘streak’ like structures in the buffer layer.

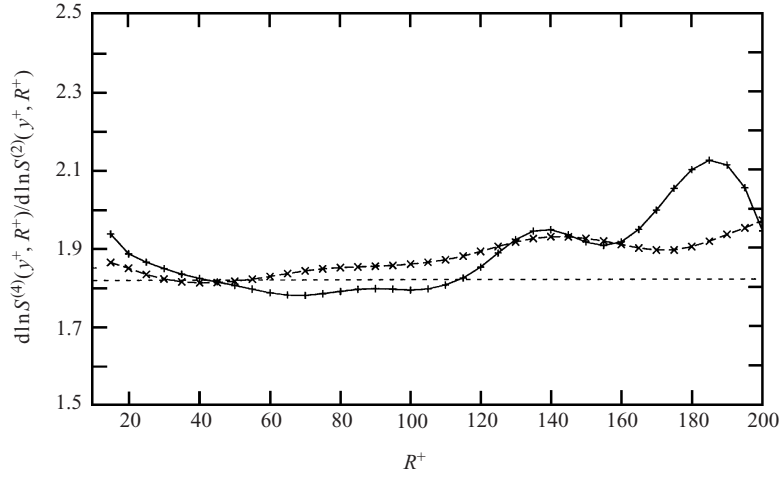


FIGURE 15. ESS logarithmic local slopes of the undecomposed structure function in the streamwise direction (+) and of the projection on the $m = 0$ sector (\times) as functions of the scale R^+ , for the moments $p = 4$ versus $p = 2$, at $y^+ = 160$. The dashed line represents the value 1.84 resulting from the experimental high-Reynolds-number isotropic measurements.

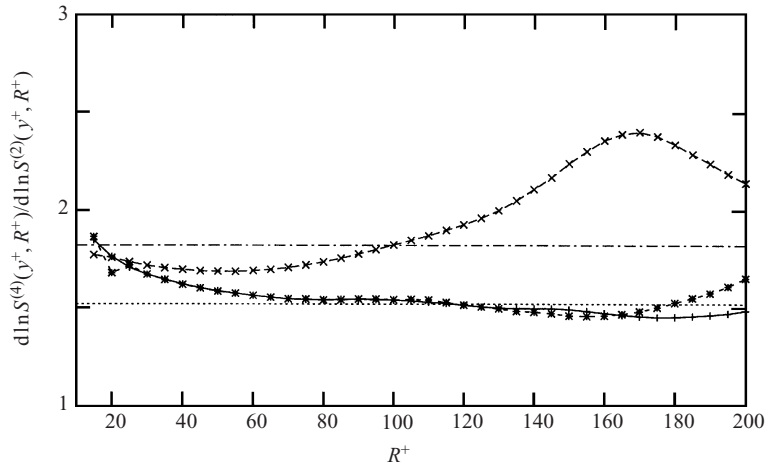


FIGURE 16. ESS logarithmic local slopes of the undecomposed structure function in the streamwise direction (+), of the projection on the $m = 0$ sector (\times), and of the reconstruction up to $m_{max} = 2$ (*) as functions of the scale R^+ , for the moments $p = 4$ versus $p = 2$, at $y^+ = 37$. The dotted line represents the best fit value, 1.52, for the ESS logarithmic local slopes of the undecomposed structure function in the streamwise direction, the dotted-dashed line corresponds to the high-Reynolds-number experimental isotropic value, 1.84, for the same quantity.

5. Conclusions

A detailed investigation of anisotropies in channel flows in terms of the SO(3) and SO(2) decomposition of structure functions has been presented. Projections on the eigenfunctions of the two symmetry groups can be seen as a systematic expansion of structures as a function of their scale and in terms of their local degree of anisotropy.

This tool may be thought of as complementary to the POD approach (proper orthogonal decomposition, see e.g. Pope 2000) where projections are made on structures specific to the flow. The advantage of the SO(3)/SO(2) decomposition as compared to

POD is that the modes on which we project are more familiar and obey the symmetry of the Navier–Stokes equations; the disadvantage is that convergence is presumably slower. Both methods share the shortcoming that hitherto they have not been proved to be useful for dynamical calculations; they are simply analysing tools.

We have used the SO(3) decomposition of structure functions at the centre and at a quarter of the channel in order to have a tool to measure the relative importance of isotropic and anisotropic fluctuations at all scales. Close to the wall, the anisotropic fluctuations show strong effects induced by structure with the typical orientations of hairpin vortices. A partial lack of isotropization is still detected at the smallest resolved scales.

The SO(2) decomposition in planes parallel to the walls allowed us to access also the regions close to the wall. In those regions, we have found that the strong enhancement of intermittency can be understood in terms of streaklike structures and their signatures in the $m = 2$ and $m = 4$ modes of the SO(2) decomposition.

We need still to understand the physics of the anisotropic flow structures and why they are more intermittent. However, we are confident that the SO(3) and SO(2) decompositions are a useful systematic tool to analyse any isotropic/anisotropic two-dimensional/three-dimensional turbulent data. We hope that in the long run, characterizations of anisotropic behaviour like the present one may help to improve LES of strongly anisotropic and inhomogeneous flows.

We thank I. Arad, B. Eckhardt and I. Procaccia for helpful discussions. The work is part of the research program of the Stichting voor Fundamenteel Onderzoek der Materie (FOM), which is financially supported by the Nederlandse Organisatie voor Wetenschappelijk Onderzoek (NWO). This research was also supported in part by the European Union under contract HPRN-CT-2000-00162 and by the National Science Foundation under grant no. PHY94-07194 and we thank the Institute of Theoretical Physics in Santa Barbara for its hospitality.

Appendix

In this Appendix, we want to explicitly write down the SO(3) decomposition of the most general two-point velocity correlations in anisotropic turbulence. We consider the second-order tensor involving velocities at two distinct points \mathbf{x} and $\mathbf{x} + \mathbf{R}$:

$$C^{\alpha\beta}(\mathbf{R}) \equiv \langle u^\alpha(\mathbf{x})u^\beta(\mathbf{R} + \mathbf{x}) \rangle, \quad (\text{A } 1)$$

where we have supposed that the statistics are homogeneous (but not isotropic) and therefore the left-hand side of (A 1) depends only on \mathbf{R} , the distance between the two points. Then, we can decompose $C^{\alpha\beta}$ according to the irreducible representation of the SO(3) group. Each irreducible representation will be composed of a set of functions labelled with the usual indices $j = 0, 1, \dots$ and $m = -j, \dots, +j$ corresponding to the total angular momentum and to the projection of the total angular momentum on an arbitrary direction, respectively. Moreover, a new ‘quantum’ index q which labels different irreducible representations will be necessary. There are only $q = 1, \dots, 9$ irreducible representations of the SO(3) groups in the space of two-indices tensors depending continuously on a three-dimensional vector (Arad *et al.* 1999b). In particular, for fixed j and m , the 9 basis tensors can be constructed starting from the scalar spherical harmonics $Y_{j,m}(\hat{X})$ plus successive application of the two isotropic operators R_x and ∂_β in order to saturate the correct number of tensorial indices. For example, the 9 linearly independent basis vectors which define the irreducible

representations (2.2) can be chosen as:

$$\begin{aligned}
 B_{1,jm}^{\alpha\beta}(\hat{\mathbf{R}}) &\equiv R^{-j} \delta^{\alpha\beta} \Phi_{jm}(\mathbf{R}), \\
 B_{2,jm}^{\alpha\beta}(\hat{\mathbf{R}}) &\equiv R^{-j-2} R^\alpha R^\beta \Phi_{jm}(\mathbf{R}), \\
 B_{3,jm}^{\alpha\beta}(\hat{\mathbf{R}}) &\equiv R^{-j} [R^\alpha \partial^\beta - R^\beta \partial^\alpha] \Phi_{jm}(\mathbf{R}), \\
 B_{4,jm}^{\alpha\beta}(\hat{\mathbf{R}}) &\equiv R^{-j-1} \epsilon^{\alpha\beta\mu} R_\mu \Phi_{jm}(\mathbf{R}), \\
 B_{5,jm}^{\alpha\beta}(\hat{\mathbf{R}}) &\equiv R^{-j+2} \partial^\alpha \partial^\beta \Phi_{jm}(\mathbf{R}), \\
 B_{6,jm}^{\alpha\beta}(\hat{\mathbf{R}}) &\equiv R^{-j+1} [\epsilon^{\beta\mu\nu} R_\mu \partial_\nu \partial^\alpha + \epsilon^{\alpha\mu\nu} R_\mu \partial_\nu \partial^\beta] \Phi_{jm}(\mathbf{R}), \\
 B_{7,jm}^{\alpha\beta}(\hat{\mathbf{R}}) &\equiv R^{-j} (R^\alpha \partial^\beta + R^\beta \partial^\alpha) \Phi_{jm}(\mathbf{R}), \\
 B_{8,jm}^{\alpha\beta}(\hat{\mathbf{R}}) &\equiv R^{-j-1} [R^\alpha \epsilon^{\beta\mu\nu} R_\mu \partial_\nu + R^\beta \epsilon^{\alpha\mu\nu} R_\mu \partial_\nu] \Phi_{jm}(\mathbf{R}), \\
 B_{9,jm}^{\alpha\beta}(\hat{\mathbf{R}}) &\equiv R^{-j+1} \epsilon^{\alpha\beta\mu} \partial_\mu \Phi_{jm}(\mathbf{R}),
 \end{aligned}$$

where $\Phi_{jm}(\mathbf{R}) \equiv R^j Y_{jm}(\hat{\mathbf{R}})$. The most general second-order tensor like (A 1) can be decomposed as:

$$C^{\alpha\beta}(\mathbf{R}) \equiv \sum_{j,m} \sum_{q=1}^9 a_{q,jm}(R) B_{q,jm}^{\alpha\beta}(\hat{\mathbf{R}}), \quad (\text{A } 2)$$

where now the physics of the anisotropic statistical fluctuations must be analysed in terms of the projections $a_{q,jm}(R)$ into the different sectors. Not all projections are statistically independent. For example, there exists the well-known constraint induced by the continuity equation for the only two projections alive in the isotropic homogeneous sector, $a_{1,00}(R), a_{2,00}(R)$,

$$R \frac{d}{dR} a_{1,00}(R) + R \frac{d}{dR} a_{2,00}(R) + 2a_{2,00}(R) = 0.$$

The above constraint has the immediate consequence that both projections must have the same scaling behaviour in the inertial range.

The continuity equation is not enough to impose similar constraints on the scaling behaviour in the anisotropic sectors $j > 0$. In the latter case, the number of constraints is less than the possible scaling degrees of freedom and therefore the possibility of having different scaling for different irreducible representations within the same jm sector is not ruled out (see Appendix of Arad *et al.* 1999b). Also, dynamical constraints like the famous Kolmogorov $\frac{4}{5}$ -law which connects the third-order longitudinal structure function with the dissipation are only known for the isotropic case. Hitherto, no exact dynamical relation of this type could be established in the anisotropic $j > 0$ sectors. The only exception known to us is the case of isotropic but non-parity invariant flow where a helicity-flux may exist in the system. In that case, for the non-parity invariant but isotropic third-order correlation functions involved in the helicity flux we can establish a relation similar to the $\frac{4}{5}$ -law (Chkhetiani 1996; L'vov, Podivilov & Procaccia 1997).

REFERENCES

- AMATI, G., SUCCI, S. & PIVA, R. 1997 Massively parallel lattice-Boltzmann simulation of turbulent channel flow. *Intl J. Mod. Phys. C* **8**, 869–877.
- ARAD, I., BIFERALE, L., MAZZITELLI, I. & PROCACCIA, I. 1999a Disentangling scaling properties in anisotropic and inhomogeneous turbulence. *Phys. Rev. Lett.* **82**, 5040–5043.

- ARAD, I., DHURVA, B., KURIEN, S., L'VOV, V. S., PROCACCIA, I. & SREENIVASAN, K. R. 1998 Extraction of anisotropic contributions in turbulent flows. *Phys. Rev. Lett.* **81**, 5330–5333.
- ARAD, I., L'VOV, V. & PROCACCIA, I. 1999*b* Correlation functions in isotropic and anisotropic turbulence: the role of the symmetry group. *Phys. Rev. E* **59**, 6753–6765.
- BENZI, R., AMATI, G., CASCIOLA, C. M., TOSCHI, F. & PIVA, R. 1999 Intermittency and scaling laws for wall bounded turbulence. *Phys. Fluids* **11**, 1284–1286.
- BENZI, R., BIFERALE, L., CILIBERTO, S., STRUGLIA, M. V. & TRIPICCIONE, R. 1996*a* Generalized scaling in fully developed turbulence. *Physica D* **96**, 162–181.
- BENZI, R., CILIBERTO, S., TRIPICCIONE, R., BAUDET, C., MASSAIOLI, F. & SUCCI, S. 1993 Extended self-similarity in turbulent flows. *Phys. Rev. E* **48**, R29–R32.
- BENZI, R., STRUGLIA, M. V. & TRIPICCIONE, R. 1996*b* Extended self-similarity in numerical simulations of three-dimensional anisotropic turbulence. *Phys. Rev. E* **53**, R5565–R5568.
- BIFERALE, L. & TOSCHI, F. 2001 Anisotropic homogeneous turbulence: hierarchy and intermittency of scaling exponents in the anisotropic sectors. *Phys. Rev. Lett.* **86**, 4831–4834.
- CHKHETIANI, O. 1996 On the third moments in helical turbulence. *Sov. Phys., J. Exp. Theor. Phys. Lett.* **63**, 808–812.
- FRISCH, U. 1995 *Turbulence*. Cambridge University Press.
- GARG, S. & WARHAFT, Z. 1998 On the small scale structure of simple shear flow. *Phys. Fluids* **10**, 662–673.
- GAUDIN, E., PROTAS, B., GOUJON-DURAND, S., WOJCIECHOWSKI, J. & WESFREID, J. E. 1998 Spatial properties of velocity structure functions in turbulent wake flows. *Phys. Rev. E* **57**, R9–R12.
- GROSSMANN, S., VON DER HEYDT, A. & LOHSE, D. 2001 Scaling exponents in weakly anisotropic turbulence from the Navier–Stokes equation. *J. Fluid Mech.* **440**, 381–390.
- GROSSMANN, S., LOHSE, D., L'VOV, V. & PROCACCIA, I. 1994 Finite size corrections to scaling in high Reynolds number turbulence. *Phys. Rev. Lett.* **73**, 432–435.
- GROSSMANN, S., LOHSE, D. & REEH, A. 1997 Application of extended-self-similarity in turbulence. *Phys. Rev. E* **56**, 5473–5478.
- GROSSMANN, S., LOHSE, D. & REEH, A. 1998 Scaling of the irreducible SO(3)-invariants of velocity correlations in turbulence. *J. Statist. Phys.* **93**, 715–724.
- HEAD, M. R. & BANDYOPADHYAY, P. 1981 New aspects of turbulent boundary layer structure. *J. Fluid Mech.* **107**, 297–338.
- KIM, H. T., KLINE, S. J. & REYNOLDS, W. C. 1971 The production of turbulence near a smooth wall in a turbulent boundary layer. *J. Fluid Mech.* **50**, 133–160.
- KIM, J. & MOIN, P. 1986 The structure of the vorticity field in turbulent channel flow. Part 2. Study of ensemble-averaged fields. *J. Fluid Mech.* **162**, 339–363.
- KLINE, S. J., REYNOLDS, W. C., SCHRAUB, F. A. & RUNSTADLER, P. W. 1967 The structure of turbulent boundary layers. *J. Fluid Mech.* **30**, 741–773.
- KOLMOGOROV, A. N. 1941 The local structure of turbulence in incompressible viscous fluid for very large Reynolds numbers. *C. R. Acad. Sci. USSR* **30**, 299–303.
- KURIEN, S., L'VOV, V. S., PROCACCIA, I. & SREENIVASAN, K. R. 2000 Scaling structure of the velocity statistics in atmospheric boundary layers. *Phys. Rev. E* **61**, 407–421.
- KURIEN, S. & SREENIVASAN, K. R. 2001*a* Measures of anisotropy and the universal properties of turbulence. *Les Houches Summer School Proceedings*, pp. 1–60, Springer and EDP-Sciences, (in press).
- KURIEN, S. & SREENIVASAN, K. R. 2001*b* Anisotropic scaling contributions to high-order structure functions in high-Reynolds-number turbulence. *Phys. Rev. E* **62**, 2206–2212.
- LUMLEY, J. L. 1967 Similarity and the turbulent energy spectrum. *Phys. Fluids* **10**, 855–858.
- L'VOV, V., PODIVILOV, E. & PROCACCIA, I. 1997 Exact results for the third order correlation of velocity in turbulence with helicity. *chao-dyn* 9705016, unpublished. The Weizmann Institute of Science, Rehovot, 76100 Israel.
- MOIN, P. & KIM, J. 1985 The structure of the vorticity field in a turbulent channel flow. Part 1. Analysis of the instantaneous fields and statistical correlations. *J. Fluid Mech.* **155**, 441–464.
- MONIN, A. S. & YAGLOM, A. M. 1975 *Statistical Fluid Mechanics*. MIT Press.
- ONORATO, M., CAMUSSI, R. & IUSO, G. 2000 Small scale intermittency and bursting in a turbulent channel flow. *Phys. Rev. E* **61**, 1447–1454.
- POPE, S. B. 2000 *Turbulent Flows*. Cambridge University Press.

- PUMIR, A. 1996 Turbulence in homogeneous shear flows. *Phys. Fluids* **8**, 3112–3127.
- PUMIR, A. & SHRAIMAN, B. I. 1995 Persistent small scale anisotropy in homogeneous shear flows. *Phys. Rev. Lett.* **75**, 3114–3117.
- SCHUMACHER, J. & ECKHARDT, B. 2001 Evolution of turbulent spots in a parallel shear flow. *Phys. Rev. E* **63**, 046307-1–046307-9.
- TOSCHI, F., AMATI, G., SUCCI, S., BENZI, R. & PIVA, R. 1999 Intermittency and structure functions in channel flow turbulence. *Phys. Rev. Lett.* **82**, 5044–5047.
- TOSCHI, F., LÉVÊQUE, E. & RUIZ-CHAVARRIA, G. 2000 Shear effects in non-homogeneous turbulence. *Phys. Rev. Lett.* **85**, 1436–1439.
- WALLACE, J. M., ECKELMANN, H. & BRODKEY, R. S. 1942 The wall region in turbulent shear flow. *J. Fluid Mech.* **54**, 39–48.